INFLUENCE OF ALUMINUM OXIDE NANOFUEL ADDITIVE ON THE SPRAY PERFORMANCE OF CONVENTIONAL AND ALTERNATIVE JET FUELS AT HIGH AMBIENT CONDITIONS

An Undergraduate Research Scholars Thesis

by

ALREEM RASHID ABDULLA AL-DOSARI

Submitted to the Undergraduate Research Scholars program at
Texas A&M University
in partial fulfillment of the requirements for the designation as an

UNDERGRADUATE RESEARCH SCHOLAR

Research Advisor: Dr. Reza Sadr
Research Laboratory Advisor: Dr. Kumaran Kannaiyan

May 2019

Major: Petroleum Engineering

TABLE OF CONTENTS

ABSTRACT

Influence of Aluminum Oxide Nanofuel Additives on the Spray Performance of Alternative and Conventional Jet Fuels at High Ambient Conditions

AlReem Rashid Abdulla Al-Dosari
Department of Petroleum Engineering
Texas A&M University at Qatar

Research Advisor: Dr. Reza Sadr
Research Laboratory Advisor: Dr. Kumaran Kannaiyan
Department of Mechanical Engineering
Texas A&M University at Qatar

The increasing demand of air transport has been driving the research interest to reduce the environmental impact of jet fuels combustion. Therefore, in addition to exploring the synthetic alternative jet fuels, nanometer-sized metal particles are added to enhance the combustion process and mitigate emissions. Studies have shown that nanofuel additive exhibit positive impact when compared to micrometer sized fuel additive in terms of combustion properties. Since the nanofuel (i.e., liquid fuel with dispersed nanoscale additives) is still in the pilot phase, the publications that studied the atomization process at elevated ambient conditions for jet fuel are scarce. Thus, the aim of the research is to study the effect of nanofuel additives on the spray performance at ambient conditions similar to the aviation combustion chamber conditions. The nanoscale additive used in this study is Aluminum Oxide (Al_2O_3) at two weight concentrations (2&4 wt.%,). The spray performance of alternative jet fuel (Gas-to-Liquid, GTL) will be compared with and without the dispersion of nanoscale additive. The GTL fuel spray performance is compared with the conventional jet fuel (Jet A-1) and the blend of GTL and Jet A-1 fuels at 50-50% by volume. This project has three major parts: Nanofuel preparation, spray experiments, images analysis. Finally, critical parameters of the spray performance are obtained and analyzed to draw conclusions.

ACKNOWLEDGEMENTS

First of all, I would like to thank Qatar National Research Fund (One of the members of Qatar Foundation) for the grant they provided to do this research project under the Undergraduate Research Experience Program (UREP); with grant ID of [UREP21-098-044.] Also, I would like to thank and acknowledge Shell (Qatar Shell Research & Technology Center) and Q-Jet for providing both types of jet fuels needed in this study.

Second of all, I would like to thank both my advisors Prof. Reza Sadr and Dr. Kumaran Kannaiyan for all their efforts, guidance, and time they provided to me to learn the basics of research, and complete the whole project, and that was a great hands-on experience for me to learn from.

Finally, I would like to thank the undergraduate students, Mohamed Soltan and Buthaina Al Abdulla, for their contribution and working with me in the initial UREP project, which I was able to extend it with six more fuel samples to study and produce this thesis.

NOMENCLATURE

IATA	International Air Transport Association
SPK	Synthetic Paraffinic Kerosene
AJF	Alternative Jet Fuels
GTL	Gas-to-Liquids
HPHT	High-Pressure High-Temperature
PID	Proportional-Integral-Derivative
MNP	Metallic Nanoparticle
AGP	Ambient Gas Pressure
NF	Nanofuel
QNRF	Qatar National Research Fund

CHAPTER I

INTRODUCTION

The Increase of Aviation Emissions

The global aviation is a demand-driven industry that serves the rapid growth of civilizing populations. Aviation transportation reports by International Air Transport Association (IATA) indicated that 53.9 million metric tons of cargo, along with over 3 billion passengers were transported in 2016 [1]. Annual reports by IATA quantified the commercial aviation activities in 2016 to be 67.6 million transportation jobs, and those are expected to go up dramatically to 90 million jobs by 2034 [1].

Today, the aviation sector contributes about 2.6% of the annual global carbon dioxide emissions [2]. Now with the projected increase of the air transportation activities, the annual aviation contribution to the global CO_2 emissions is expected to increase up to approximately 20% by mid-century [2]. Meanwhile, there is an increasing awareness of the aviation fuel combustion anthropogenic, such as greenhouse gas emissions and climate change. Thus, several strategies, studies, regulations were made seeking the mitigations of greenhouse gas emissions by providing cleaner fuels and innovative technologies [1-3].

New Technologies/Solutions

Conventional and Synthesized Jet Fuels

In general, the conventional aviation fuel is a petroleum-based liquid, which is made specially to operate on gas turbine engines. The aviation fuels quality is very restricted when compared to that of ground transportation fuels [4]. Some of the main aviation fuels criteria are: high energy content, satisfactory flow characteristic and thermal stability [5,6].

Two of the common conventional civil aviation jet fuels, Jet A and Jet A-1, are kerosene-based fuels derived from crude oil [7,8]. Those fuels met the engines' required fuel specifications; such as: maximum allowable deposits in standard heating tests, maximum allowable freeze point temperature, acceptable minimum energy density by mass, maximum allowable sulfur and aromatics content, maximum allowable viscosity, etc. [4].

Nevertheless, with the world's increasing interest towards Alternative Jet Fuels (AJF), as they proved to be prominent surrogate for the oil-based fuels, the transition should preserve the above-mentioned specification, due to existing engines requirement. Synthetic Paraffinic Kerosene (SPK), synthesized from natural gas through Fischer–Tropsch process, is a one of the promising AJF that paved its way to the aviation industry. For instance, natural gas can be converted to liquid fuel via this process, and it is called Gas-to-Liquid (GTL) jet fuel. It proved its efficiency in terms of providing cleaner combustion and mitigating engine emissions [10,11].

Nanoscale Metal Additives

Despite the progress of producing renewable sources-based jet fuels via many processes by the use of various bio-feedstocks [10], researches and studies are carried on seeking the goal of finding innocuous jet fuel. As the evolution of renewable alternative jet fuels might take longer time to be fully implemented in the industry, new methods to improve the performance of the currently used drop-in fuels are still under research. One of those emerging methods is the idea of adding metal particles as fuel additives. The goal of the dispersed micrometer-sized energetic (i.e. acquiring high energy to volume ratio) metal particles in the liquid fuel is to enhance the heat release in the fuel combustion, and thereby, lessen the particle matter and emissions end-product [12]. This innovation started with what is called Slurry Fuel; defined as micron-sized metal particles dispersed in fuel carrier, in high concentrations ranging between 50-80 %. Several

metallic particles are used in this technique; however, it was found that Aluminum, Boron and Carbon were the commonly used particles [12-14]. Studies have shown that slurry fuels have better combustion efficiency; yet the used additives increased the ignition time delay with other undesired outcomes [13-16]. Thereafter, the advent of nanotechnology introduced the metal and metal oxide nanoparticles. These smaller (when compared to micrometer sized) particles revived the concept of metal particles dispersion in jet fuels as performance enhancement additives. Several studies were conducted to gain sound knowledge regarding the effects of the nanometer-sized fuel additives.

Literature Survey

The similarity between the micro-scale and the nano-scale additives is the concept of high energy density or high surface to volume ratio. Meaning that those particles are very interactive in terms of thermochemical reactions, yet their intensity varies in terms of thermodynamics according to their sizes. This is where the nano-scale additives exhibit positive effect on the fuel performance. Starting with the thermophysical properties aspect, researches have demonstrated the enchantment made the nano-additives in terms of the heat transfer, exothermic characteristics and the fuel mixture stability [17-20]. In addition, studies have shown that the evaporation characteristics of nanofuels are improved due to the phenomenon of microexplosion, which enhances the vaporization process [21]. Other studies showed that nano-scale additives increases the energy content of the fuel, and enhances its combustion and autoignition characteristics. [22-26] Thus, these studies renewed the world's interest of the nano-scale fuel additives.

Objective of This Work

The objective of this work is to study the effect of Aluminum Oxide Nanoscale fuel additives on three macroscopic spray performance parameters, on both conventional and

alternative jet fuel and their mixture. The benefit of this work is to add vital findings to the research community database.

CHAPTER II

EXPERIMENTAL SETUP & METHODOLOGY

Spray Experimental Setup

To simulate the conditions of the gas turbine engine's combustion chamber, a state-of-the-art High-pressure High-temperature (HPHT) spray facility was built. The use of the spray facility is limited to investigate the non-reacting atomization properties. *It is important to mention that this work is an extension of our UREP work (Soltan, et al. 2018) and all details of the built facility presented in this section, and the part of the methodologies used here were fully reported by Soltan et al. 2018 [27]; based on the operational restrictions found in the literature [28,29,] along with some of work's demonstrative figures* [30]. The facility as a whole is illustrated in Figure 1 [27].

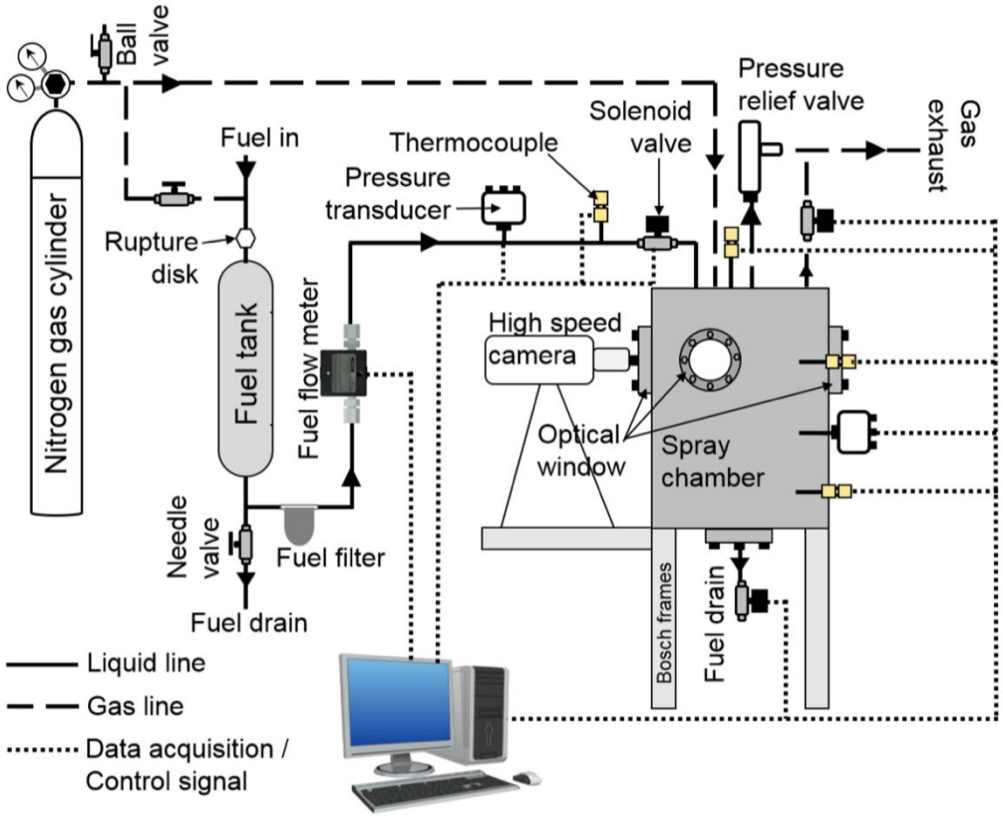

Figure 1: Schematic illustrating the built spray experiment facility [27,30].

The spray chamber was developed following the pressure vessel regulations set by ASME-section VIII, Division 2 code, with a general safety factor of four. When the chamber was in the designing stage, it was designed to resist high temperatures and pressures, however, the operating conditions of the chamber are restricted by the presences of optical windows. As for measurements, the chamber's wall thickness, and the optical windows thickness were 3.125, and 2.25 inch, respectively. These dimensions were selected to be much higher than the suggested thickness by Pipe and Shell design catalog for safety purposes. The chamber can function safely under maximum pressure and temperature conditions of 2.5 MPa and 450 K, respectively. These conditions are applicable even with the presences of the optical window. The chamber has four optical windows made of quartz, each has a viewing diameter of 75 mm. The optical windows are inserted into the chamber's design in order to allow light access on one side in which the spray shadow will be casted on the counter window. The casted spray shadow will be captured and analyzed to evaluate the fuel's spray performance. Also, the bottom of the chamber, shown in Figure 2, has the ability to mount another optical window to provide spray cross-sectional view, in case it was required.

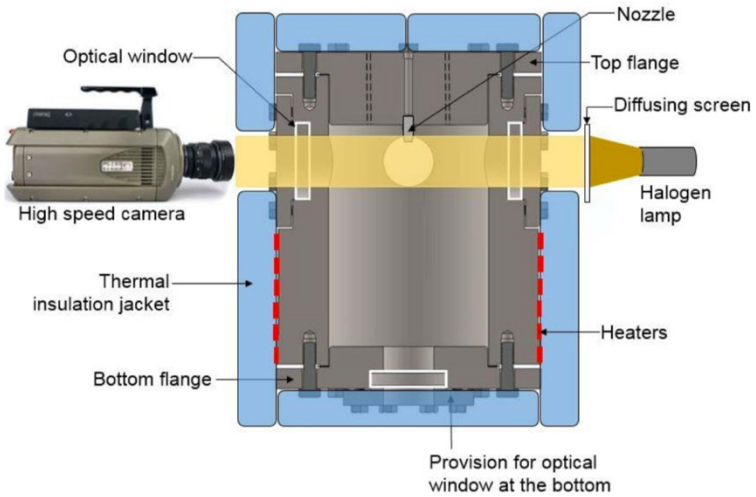

Figure 2: Illustration of the spray chamber with optical components arrangement [27,30].

The study of the spray performance was done with the presence of inert gas (i.e. Nitrogen) inside the chamber to provide pressure, and it was used to prevent any incidents of combustion or ignition that might threat the safety of the process. The inert nitrogen gas was injected into the chamber via a non-returning valve at the top of the chamber. By the amount of gas injected into the system, the chamber's pressure was controlled. The pressure of the chamber was monitored closely during experimentation by the use of pressure transducer (Setra Model 207, USA) placed on outside of the chamber (see Figure 1). For controlling the gas temperature inside the chamber, band heaters were coiled around the outer side of the chamber, at the bottom part only. While on the top part, patch heaters were used as they accommodate the existence of optical windows, unlike the band heaters.

The specifications of both band and patch heaters are listed below in terms of heat flux, and the manufacturer name:

- Band Heater: 8.6 W/in^2, Omega Engineering, USA.
- Patch Heater: 5 W/in^2, Omega Engineering, USA.

Moreover, T-type thermocouples from the same manufacturer were used to monitor the temperature at three part of the system: top, bottom, and near the nozzle. The thermocouples were connected to a software called LabView for viewing the generated data and observe them on a continuous manner. In addition, the system was connected to Proportional-Integral-Derivative (PID) as a heat controller. Since there were two types of heaters (band and patch), two PID's were added to the system to control each type individually.

The top flange of the chamber has three ports : first for gas exhaust line, second for pressure relief valve, and the last one for thermocouples. The importance of the top's thermocouple is that it takes readings of the chamber's temperature; and the temperature near the nozzle as well. There

are 5 main lines/streams: gas exhaust line, gas exhaust from the chamber, gas supply to the chamber, fuel supply to the nozzle, and the liquid drainage out of the chamber, all are being operated by solenoid valves. Furthermore, one line that is directly connected to the spray nozzle is the fuel line. It is critical to measure fuel's pressure, temperature, flowrate as it flows. Hence, a pressure transducer, thermocouple and a flowmeter were mounted on the fuel supply line. The temperature of the fuel line was set and maintained at 288 K during all spray experiments. The fuel line connects the spray chamber to the fuel source, which in this case is the fuel vessel by Swagelok, and, it can hold pressurized liquids up to 12 MPa. The vessel is set with a rupture disk at the line that connects the vessel with the nitrogen tank to provide means of safety.

As mentioned above the spray performance will be evaluated by the spray's shadow, and this technique is called shadowgraph. In order to apply this technique, the alignments of the optical windows, high speed camera, and Halogen lamp are taken into consideration. To illustrate how the alignment is done and how shadowgraph images will be created and gathered, a cross-sectional view of the chamber along with shadowgraph technique is presented in Figure 2.

To ensure high levels of safety, the built spray facility was surrounded by ballistic grade Kevlar boards (i.e. bullet proof) from four sides, and it was activated and managed from the outside. The whole spraying chamber was covered by thermal insulation coat of 2 inches thick

made of fiberglass. On top of that, it was bounded by Kevlar fabric covering the metal wire assembly on the thermal coat. Finally, Figure 3 shows a photograph of the spray facility [30].

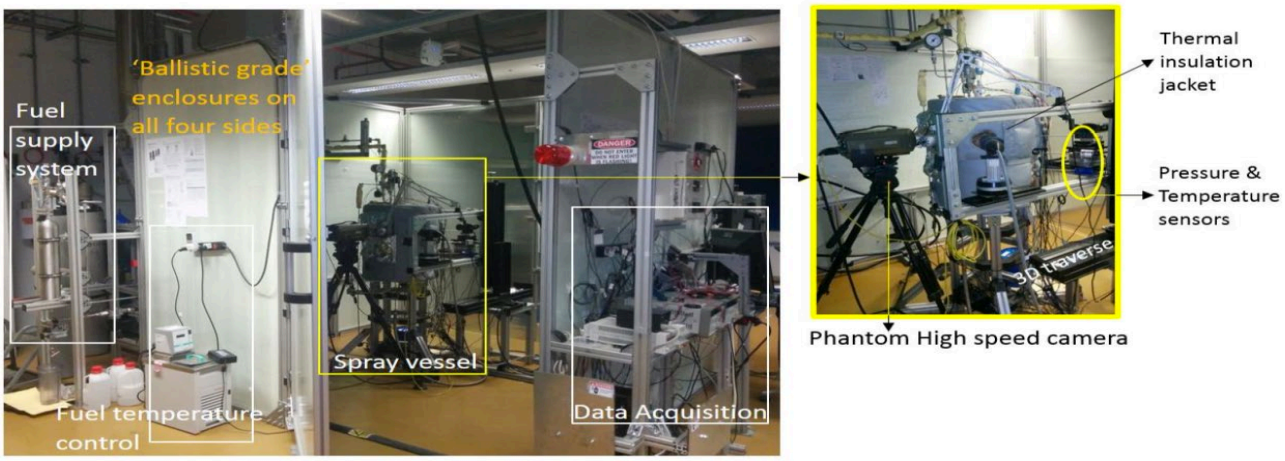

Figure 3: A photograph of the spray experiment facility [30].

Before beginning of the experimentation stage, several vital parameters have to be determined, and those are referred as the high ambient conditions. It was desired to simulate the actual combustion chamber conditions; however, it was unreachable in this work due to several restriction of safety and maximum limits of the built facility [28,29]. The operational factors were selected based on the literature values and the projects restricting limits. The values are presented in Table 1 [27] with other properties and relevant information.

Table 1: Operational factors values selected with other relevant information [27].

Operational factors	
Ambient gas pressures (kPa)	100, 500, 900
Ambient gas temperature (K)	400
Pressure difference across the nozzle (kPa)	300
Fuel temperature (K)	288
Reynolds number (-)	16750 ± 160
Uncertainty in pressure (kPa)	± 6
Uncertainty in Temperature (K)	± 2

All the samples in this project were tested in the spray facility at different chamber pressure settings mentioned in Table 1. Because of changing the gas pressure in the chamber, the fuel injection pressure is to be changed accordingly. So that the differential pressure across the nozzles remains at 300 kPa. The nozzle used in this spray experiment is a swirling nozzle by Duesen-Schlick, Germany. This nozzle was particularly selected as it is the common type used in commercial aviation engines [37]. The functions of this type of nozzles are initial stabilizer of the ignition and flaming stages of the process. The nozzle outlet port has a diameter (D_n) of 0.8 mm. After each experiment, the used Nitrogen was replaced with the new amount of fresh Nitrogen. This was done to avoid fuel vapor saturation. Not only the used Nitrogen was evacuated out of the chamber by the new gas but also, the liquid fuel that settles on the bottom of the chamber was drained regularly. Each set of experimentation was repeated to verify the desired outcomes. Additionally, the fuel supply line was purged with the base fuel (0 wt. %. of nanoparticles) after test a nanofuel (i.e. nanoparticles dispersed base fuel) to move out any adhered nanoparticles to

the supply line. For elaboration, to understand the flow regime inside the fuel line, the fluid's Reynolds was calculated using the Equation 1 [32]. Where $\boldsymbol{\rho}_L$ denotes fluid density and $\boldsymbol{\mu}_L$ denotes dynamic viscosity, and ΔP represents the differential pressure across the nozzle. It is important to understand the flow regime as its velocity and how it exists through the nozzle affect the spraying characteristics [33]. Lastly, the spraying experiment was conducted twice to verify the obtained outcomes.

$$\boldsymbol{Re}_p = \frac{\mathbf{Dn}\cdot\boldsymbol{\rho}\mathbf{L}}{\boldsymbol{\mu}\mathbf{L}}\sqrt{\frac{\mathbf{2}\,\Delta\mathbf{P}}{\boldsymbol{\rho}\mathbf{L}}} \quad \text{.....Equation 1}$$

Nanofuel Preparation

The goal of this project is to test the effect of Metallic Nanoparticle (MNP); Aluminum Oxide to be specific, on both conventional and alternative jet fuels. This type of MNP was selected due its compensations of the cost-benefit trade off [32]. The used Al_2O_3 MNPs have an average diameter of 13 nm, purchased from Sigma Aldrich, USA. The fuels tested in this project are Jet A-1 as the conventional jet fuel, and SPK GTL as the alternative jet fuel. For further experimentation purposes, a mixture of both fuel (50% of volume each) and evaluate the effect of the nanoparticles on the mixture. It was thought that the two jet fuels mixture might yield optimized results compromising the separated fuels properties. Each of these three fuel samples were used in creating three nanofuels samples; each sample was consisting a certain MNPs concentration. There were three MNPs concentrations to be studied: 0 (pure), 2, and 4 weight percent (wt.%). The zero concentration is denoting the base/pure fuel. The other two low concentrations were decided to avoid the creation of slurry fuels and taking into consideration other factors like prices and quantity, etc. [32]. After mixing the MNPs with the fuel, there is possibility for the particles to settle at the bottom of the container. Thus, a stable (i.e. non-settling or agglomerating) nanofuel has to be obtained by two dispersion techniques. The first one is chemical dispersion technique

conducted by adding a surfactant to the mixture. The used surfactant is sorbitan monooleate, and it is commercially known as Span80. This fluid achieves the desired dispersion by coating the nanoparticles to reduce their surface energy in which it doesn't adhere to each other and agglomerate. The surfactant was added to the mixture in a volume concentration of 0.5% and this concentration was chosen based on a stability sensitivity test done in the work of Kannaiyan et. al [32]. The selection of Span80 was done as it proved to exhibit the highest quality of separation compared to other surfactants [34]. Thereafter, the second method of dispersion was conducted to further enhance the stability of the nanoparticles. It was a mechanical separation technique in which the mixture was Ultrasonicated by using an immersion probe sonicator with the specifications of: QSonica S-4000, at 20 kHz. The sonication process lasted for 2 hours by performing in cyclic pattern to produce a stable mixture. Moreover, to lessen the formation of fuel vapor due to sonication, the temperature of the fluid was maintained to be cool by the use of a chiller from Julabo, Germany. By that, the preparation of nine nanofuels is done. Samples of the prepared nanofuels are shown in Figures 4-6.

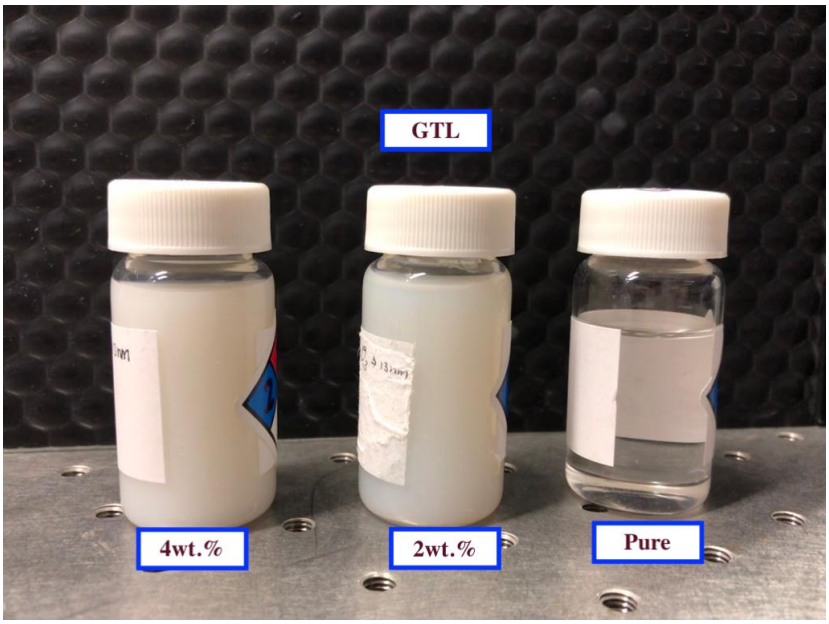

Figure 4: Nanofuel samples with a base of GTL and MNP at different concentrations.

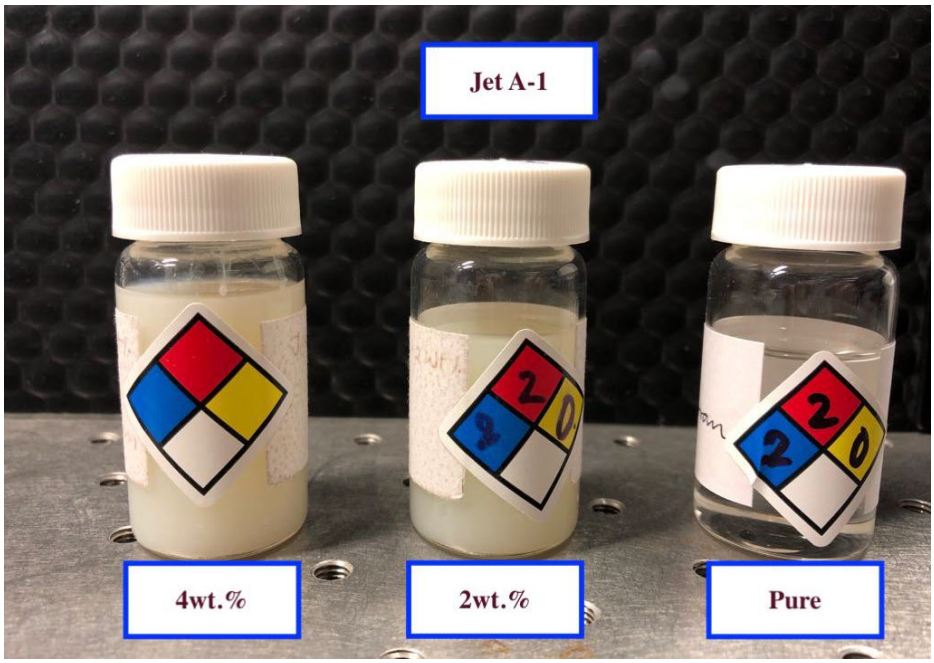

Figure 5: Nanofuel samples with a base of Jet A-1 and MNP at different concentrations.

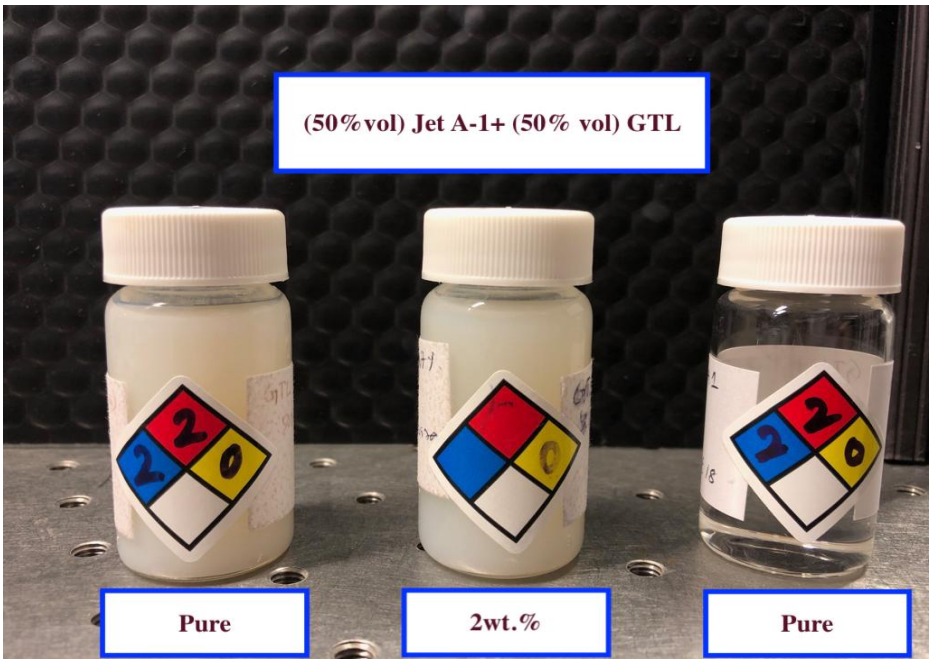

Figure 6: Nanofuel samples with a base of GTL and Jet A-1 Mixture and MNP at different concentrations.

Optical Diagnostic (Measurement) Technique: Shadowgraph and Post Processing Methodology

During the spraying experiment, pictures of the sprayed nanofuels are captured near the nozzle. This diagnostic technique of shadowgraph is shown in Figure 2. The used light source was (150 Watt, Halogen Dedo lights, Germany) positioned on one side facing the spray. On the other side, the camera, which was a high-speed camera CMOS (Vision Research Phantom v12.1), that was equipped with a macro lens of (Sigma Macro 105mm / f#5.4), was placed on the counter-side of the light sources. During the spraying experiment, the camera was functioning at an image capturing rate of 32,000 image per second, with a shutter speed of 2μs. The camera had a resolving power of 480 x 304 pixels, in which all produced images had this resolution. This quality is needed as the camera was set to capture the nozzle's outlet, in addition to the cone-shaped sprayed fuel, but only to a length of 10 mm. Furthermore, to adjust the scale of the image resolution to the reality, a factor of 34μm/pixel. More details regarding this methodology were elaborated in other paper of Kannaiyan et. al [32]. To wrap-up the camera setup, it was synchronized with the fuel supply line and, set with a trigger of 500 ms delay after the valve opening. This was done to ensure that when the fuel is supplied, it will not be activated till the flow gets sprayed.

The macroscopic characteristics of the sprayed fuels were captured by the shadowgraph images and three of those were studied here. The first one is the spray cone angle near the nozzle, that is an angle between the two edge of the cone-shaped sprayed fuel, denoted as (2θ). The second characteristic is the liquid sheet breakup distance (L) that describes the vertical space between the nozzle outlet and beginning of the liquid layers' dispersion into droplets. The third and the last characteristics is the velocity of liquid layers before their breakup. For analyzing the first two characteristics, an in-house MATLAB code was used to perform calculations in a statistiscal

approach to get the values of these two characteristics, which needed around 5000 images to do so. The same software was used to develop a tool that use the cross-correlation approach [35,36] to evaluate the third characteristic, and it needed around 1000 image pairs to do so. For the approach used in evaluating the third property, around 418 examination point were located inside the spray cone as shown in Figure 7. Each examination window is 20 x 20 pixels in size and the radius of investigations around the examination point was 60 pixels. For elaborative details upon the use of cross-correlation are found in other references [32].

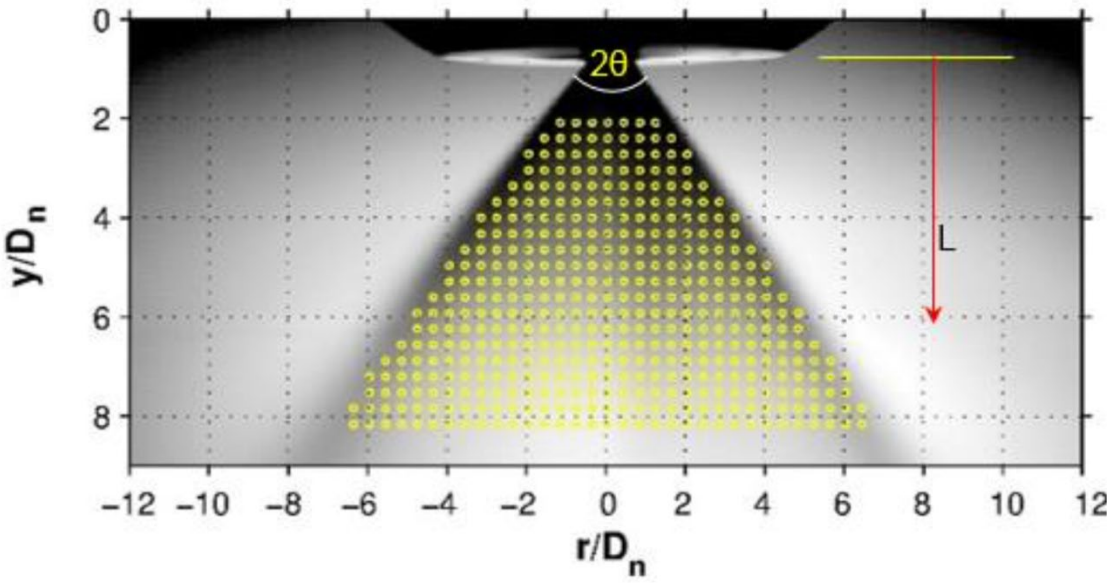

Figure 7: Overlap of the examination widows on an averaged spray image, in which the vertical distance from the nozzle the image's bottom is denoted as (y); the radius of investigation is (r), and (D_n)

CHAPTER III

RESULTS & DISCUSSION

Spray Performance

It is important to mention that in one third of the results obtained here were previously reported in (Soltan, et al. 2018) as this work is an extended version of it. The second third was presented in to the QNRF as a requirement of the research grant process, yet is was not published. Where the results of the three nanofuels (i.e. GTL and Jet A-1 mixture at three MNP concentrations) are reported for the first time [27,30]. The results of the three characteristics (Cone angle, Liquid sheet breakup distance, and the liquid sheet velocity) are reported and discussed here for the nine nanofuel samples (i.e. two jet fuels and their mixture as base fuels, in addition to MNP at three concentrations for each base fuel).

To ensure operations are conducted at high level of safety, the spraying chamber was filled with Nitrogen instead of air, as an ambient gas. So, the pressure inside the chamber is basically the pressure of the Nitrogen, which is referred to as ambient gas pressure (AGP). So the AGP changed throughout the experimentation stages, a variating parameter. However, the temperature of the chamber did not change with the changing pressure and it was kept constant at 400 K. In addition, the other parameters were temperature of the fuel supply stream at 288K and the pressure difference across the nozzle at 300 kPa for the cases presented in this section.

For comparison purposes, shadowgraph images are presented for each nanofuel in Figure 8-9 [30]. Each Figures illustrate the shadowgraph images (actual and averaged,) where each set shows the nanofuel spraying at variating AGP and MNP concentrations denoted here as NF

(nanofuel). NF=0; is the pure fuel with zero concentration of MNPs. NF=2, and NF=4 indicate the MNP concentration of 2wt.% and 4 wt.%.

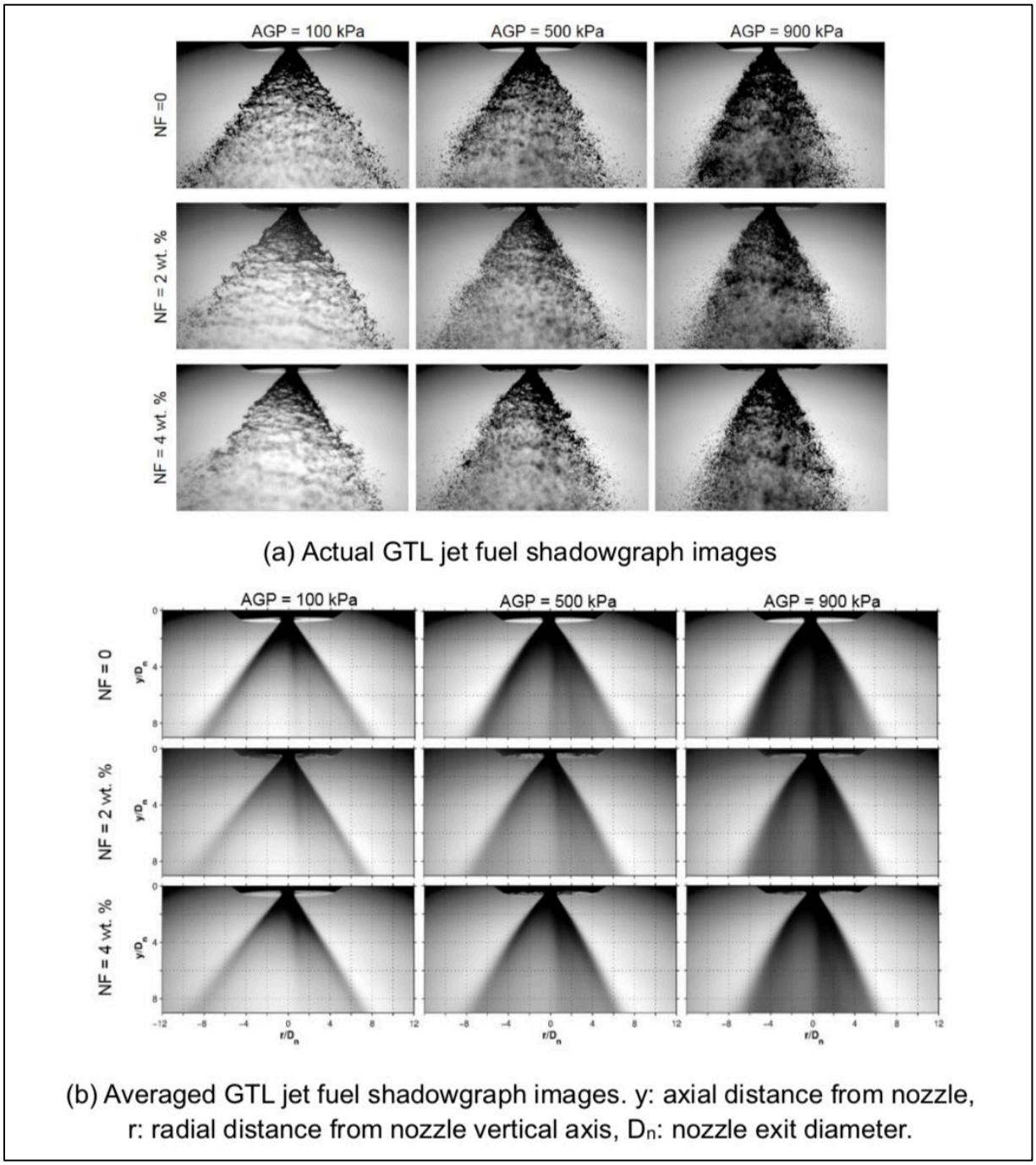

Figure 8: Representation of shadowgraph images obtained from the GTL based nanofuel at different concentrations of MNP and AGPs. Set (a) real images, (b) averaged images [30].

For the averaged images shown at the bottom part of the figure, they were averaged by the use of 5000 real images captured in progression. The cone half-angle, located near the nozzle outlet in which y/D_n is greater than 1 and less than 2.5, was almost the constant with a value of 32±2 degrees at all AGP cases for all the GTL nanfuels. Later, it was found that this constant result was because the cone angle depends on the shape/geometry dimensions of the swirling nozzle [37], which in the case of this study remained the same for all the experiments. However, as for the downstream of any nanofuel tested here, the effect of increasing the AGP was clear in the reduction in spray cone angle as it was stated for the base fuel [19]. At further distances of the downstream, the liquid sheet traveling/propagating at high velocity and starts to breakup, its droplets are being drifted towards the spray axis due to the AGP as they lose their driving force once ejected from the nozzle. Another reason for the downstream angle reduction is that the pressure at the edges of liquid spray is lower than the APG; and therefore, it concaves towards the spray axis [37]. All nanofuel and base fuels are exhibiting the same behavior of the angles (near and far from the nozzle) in terms of variating AGP.

Looking back at Figure 8, we can see the effect of increasing the MNP concentration on the cone angle for a constant AGP. However, this modest incremental increase of the MNP concentration resulted in a relatively small reduction in the cone angle. The reduction can be justified by existence of MNPs in the liquid sheet in which they caused distribution at early times. In Figure 9 the effect of AGP and different MNPs concentrations at the GTL based nanofuels is illustrated. Moreover, the images were processed by MATLAB in which the edge detection method was applied to measure the spray cone angle. The figure states there is an inversely proportional ratio between the AGP and the cone angle, and the same trends applied to the MNP concentrations. These behaviors of the cone angle with the respect of MNP concentration and AGP

are the similar for GTL and Jet A-1 base and nanofuel. The error of obtained results was calculated and it was found the deviation of the measured cone angle was typical at 95% of confidence interval [38].

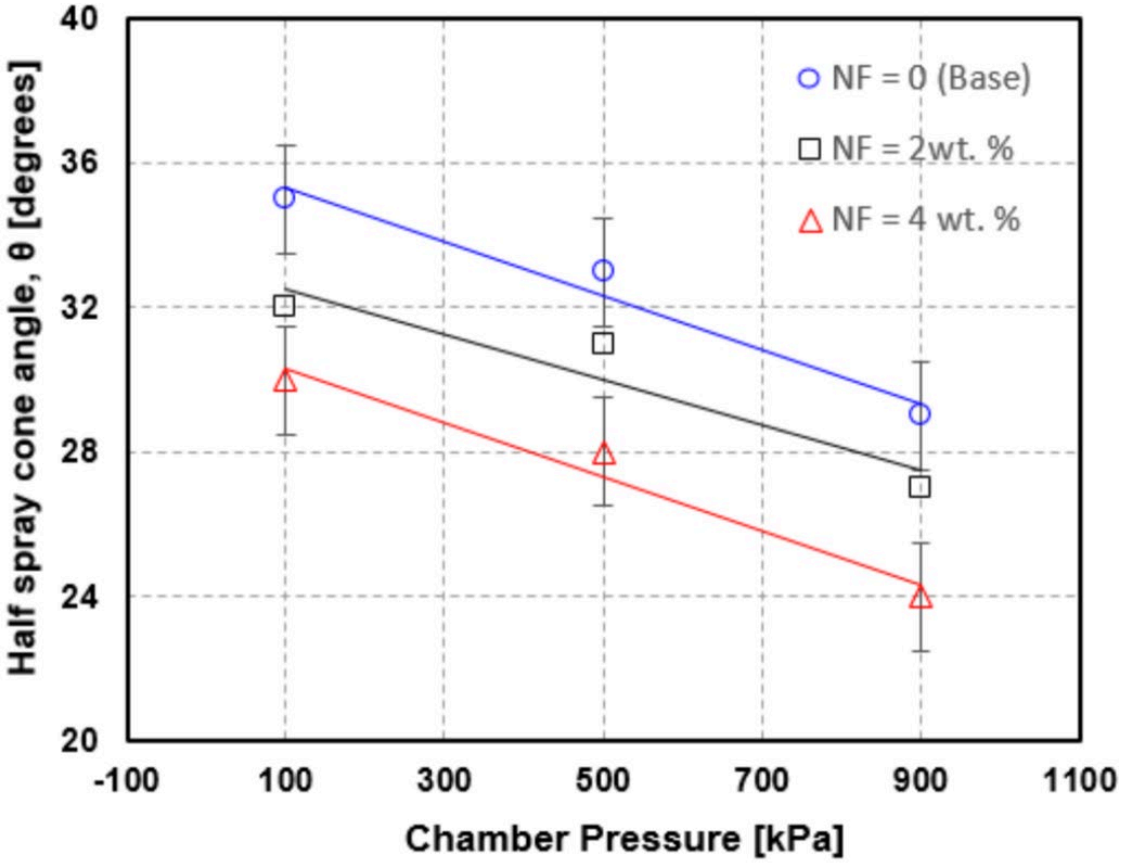

Figure 9: The results of spray cone angle as a function of MNP concentration and AGP for GTL based nanofuels [27,30]. The angle of GTL50-Jet A-1 50 is in between the pure fuels and hence not shown here.

The disruption caused by the existence of the MNPs on the liquid sheets can be studied thoroughly by applying the second order statistical moment that is the standard deviation of the real image intensities or saturation of the shadow in almost 5000 images to recognize the liquid sheet breakup dynamics [32]. The standard deviation is used here to capture the images intensities fluctuation in the spraying process. Figure 10 the vertical variation of standard deviation on image

intensity along the nozzle axis that r/D_n equals to zero. The images were normalized in terms that one initial image (i.e. no spraying) was set to be the background and all the images that comes after are result of color intensity function according to the location of liquid in the image (i.e. more liquid in a certain spot is shown by darker shades.) This is done to mitigate the effect of uneven light intensity of the image results. The highest points of the standard deviation curve implies the highest image fluctuation. Having said that, it can be concluded that the highest fluction indicates the highest liquid sheet instability. In other words, it will show the location in which the liquid sheet starts to breakup. To support the concept of using the summits of the standard deviation curves can be a good tool in identifying the liquid sheet breakup as it was founded in a previous work [32].

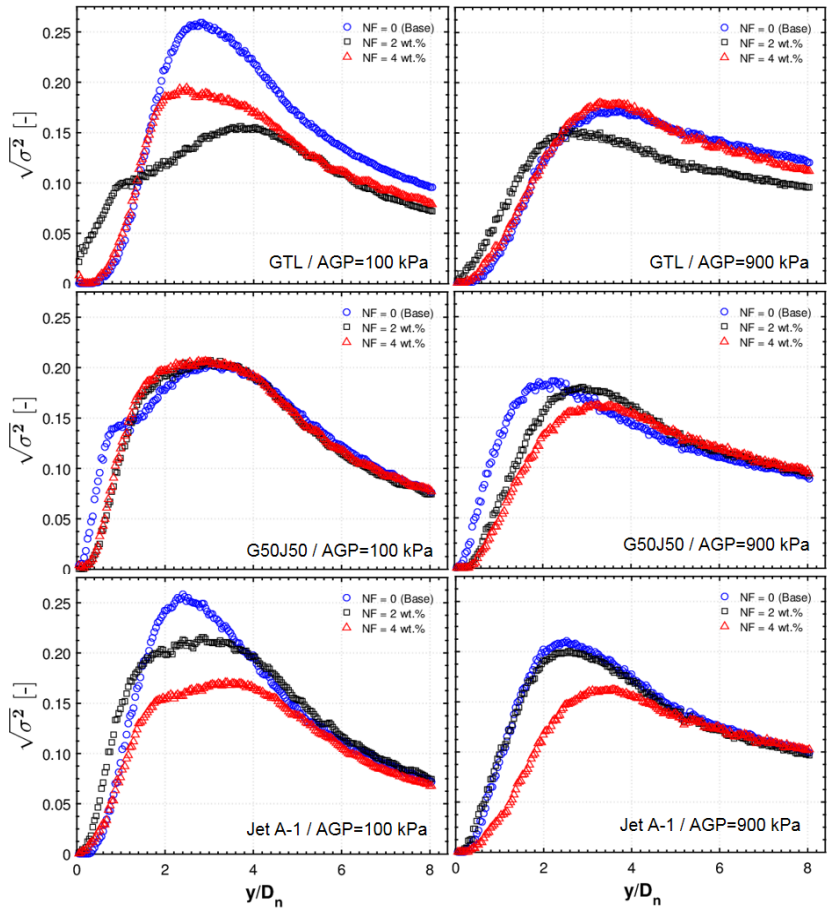

Figure 10: Standard deviation of image intensity data for base fuels: GTL, GTL50% -JetA-1 50% and Jet A-1, for different MNP concentrations at different AGP.

By looking at the Figure 10, at the GTL column with AGP equal to 100 kPA, the location of the highest point is relatively far from the nozzle's outlet for the zero MNP concentration fuel, as we compare it with two other nanofuels. Meaning that the liquid sheet breakup distance has decreased when MNP is added to the fuel. For Jet A-1 fuel at the same AGP and MNP concentration, the results were very close to each other; they exhibit the same trend and resulting in the same conclusion as the GTL case. Another point to mention here is that the standard deviation values of the nanofuels summits are lower when compared to the pure fuels. It was noticed here that the curves of the nanofuels are not showing a continuous pattern, the curves of 2wt.% resulted in standard deviation values, higher than the 4wt.%. That implies that the MNPs effect on the liquid sheet breakup properties at a certain concentration more than the other. In addition, in all the cases in Figure 10, the curves of 4wt.% always have the lowest curve values in terms of summits. This can be explained by having high concentrations of MNPs, the density and the viscosity of the nanofuel increase , meaning MNPs enhances the intermolecular adhesion; and therefore, restraining the liquid sheet from breaking up loosely. Moreover, as AGP increases, the standard deviation values are decreased, and that is justified by the reduction in the spray cone angle at the downstream and as results in lower fluctuations. Note to mention here that the curves of GTL fuels, the ones with MNPs surpassed the pure fuel at all AGPs. Nevertheless, the Jet A-1 with 2wt. % at all AGPs was similar to the pure Jet A-1, indicating that the MNP 2wt.% was not significant effect on the Jet A-1fuel performance. Another point to mention here is that the values of standard deviation in Jet A-1 at MNP concentration of 4wt.% were least in all AGP cases. This result is contrary to the 4wt.% in all AGP for GTL based fuels. So, the results are showing that GTL nanofuels experienced a notable change in liquid sheet breakup distance compared to the Jet A-1 nanofuels. The results illustrated in Figure 10 are affecting the evaporation characteristics

shown in Table 2. The table show the physical properties of the fuel sample which were reported in previous studies[27,30]. Note to mention, that physical properties of the mixture sample of GTL 50 and Jet A-1 50 were falling in between the results of the single base fuel samples. Therefore, they were not presented here.

Table 2: Physical properties of base fuels (GTL and Jet A-1) with their based nanofuels at different MNP concentrations [27,30].

Physical Properties	Nanofuel (wt.%)					
	Base Fuel (0)		2.0		4.0	
	GTL	Jet A-1	GTL	Jet A-1	GTL	Jet A-1
Density (kg/m^3) ± 2	751	788	764	799	770	816
Dynamic Viscosity (cP) ± 0.003	1.005	1.019	1.020	1.205	1.41	1.221
Surface Tension (mN/m) ± 0.07	24.1	26.9	23.2	24.8	22.8	23.2
Refractive Index(-) ± 0.003	1.417	1.439	1.419	1.441	1.421	1.445

In this study, the liquid sheet disruption happened because of the traveling of wave instability [37]. In addition, with the increase of AGP in the system, the aerodynamic drag cause to change the shape of the sprayed fuel from a flipped funnel to a solid cone, as shown in Figure 8. The hollow space of the funnel is being filled by the fuel drops compressed there because of the AGP; hence the spray shape transfer from hollow to solid cone.

For the last property to study here, the velocity which is related to the liquid sheet breakup distance. The velocity of the liquid sheets were found by using cross correlation technique on 1000 shadowgraph image pairs. This number of images where needed to find the mean axial velocity. Figure 11 is illustrating the mean axial velocity found at the nozzle's outlet and varying AGPs and MNPs concentrations for GTL and Jet A-1 based fuels. This technique is used to evaluate the spatial displacement [35] of the traveling fluid and it should provide precise data as reported in other work [36]. Additionally, the signal-to-noise ratio was improved by averaging 1000 real shadowgraph images. The maximum error in spatial displacement must not be more than half peak width; because the mean velocity at each examination window rely on it, and that is shown in the error bar at 95% confidence intervals [38].

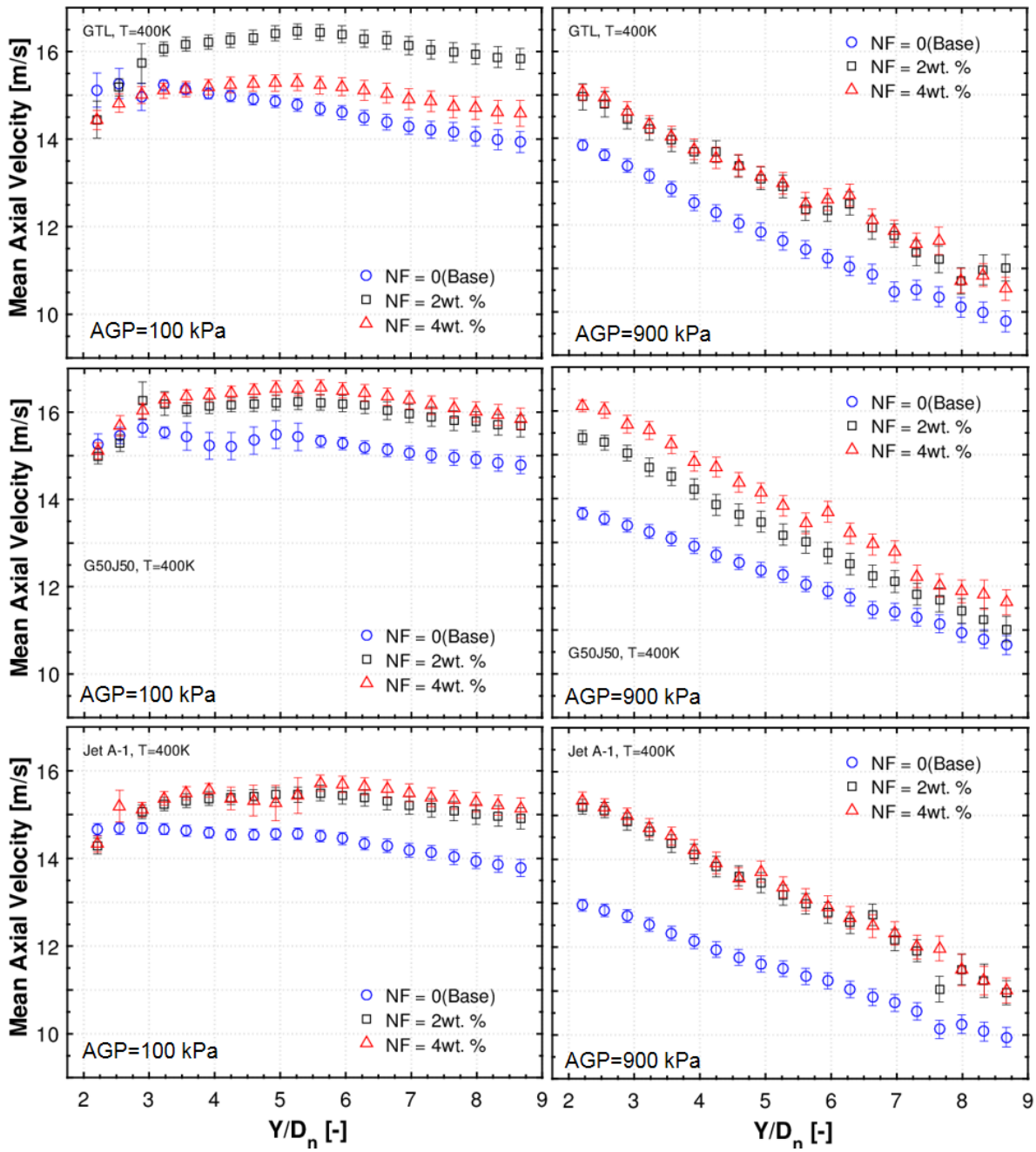

Figure 11: Mean axial velocities for base fuels: GTL, GTL50% - Jet A-1 50%, and Jet A-1, for different MNP concentrations at different AGP.

In the cases presented at the Figure 11, the drag effect reported in the literature comes into effect by reducing the liquid sheet velocity. As with the increase of AGP, the drag effect increases and reduces the liquid velocities even further. Near the nozzle at AGP of 100 kPa, the velocities

were similar for base and nanofuels. Yet, at the downstream, the GTL fuel with MNPs showed higher velocities when compared to the pure fuel, along with the increase of AGP. The same trend applies to Jet A-1, even the minor exception of this trend near the nozzle at 100 kPa AGP. Thus, the presented trends of the liquid sheet velocities are aligning with the trends shown for the liquid sheet breakup distance. So, the disturbance caused by the early mounting of instabilities in nanofuels, is contributing to the liquid sheet breakup at short distances, in which the sheet turns into droplet which travels faster. As with the increase of AGP, the formulated droplets are compressed and being pushed towards the hollow part of the funnel-shaped fuel, where they get packed and experience significant drop in velocity. At high AGP, the velocities on the edges of sprayed fuel is higher at nanofuels compared to base fuels.

To recap, the macroscopic properties of spray performance of convention and non-conventional jet fuels with the presence of Nano additives, at elevated ambient pressure, where studied and presented in this work.

CHAPTER IV

CONCLUSION

Summary of the Research Findings

In conclusion, the objective of this work was to study macroscopic spray properties for both conventional and alternative jet fuels. Those fuels were with different concentrations of Aluminum Oxide nanoparticles dispersed at different concentrations of: 0, 2, 4wt %, The fuels were sprayed inside a chamber with varying AGPs, in an attempt to simulate a real engine's combustion chamber. In addition, a mixture of both fuels (SPK GTL & Jet A-1) were subjected to the experimentation. The three studied properties are the cone angle near the nozzle, the liquid sheet, breakup distance and the liquid sheet velocity. To study those properties, shadowgraph imaging technique with a high-speed camera was used. Subsequently, the produced images were analyzed by using MATLAB that measured the properties using two different statistical approaches. The results are presented as follows:

- Near the nozzle's outlet, the cone angle remained similar for tested fuels at all AGPs, and MNP concentrations. This is because the cone angle was mainly effected by the geometry of the nozzle, which in this study was the same for all cases.
- When the fuel is sprayed from the nozzle it forms a shape of the flipped funnel (i.e. almost empty from the inside with the exception of few droplets). When the AGP is increased it compresses the liquid sheets, in which the droplets are drifted towards the center of the cone. This behavior was seen in all fuels of different bases and MNP concentrations.

- At each AGP, the nanofuel showed a slight reduction in the cone angle compared to base fuels (i.e. zero MNP concentration). Yet, these results are found within the range uncertainty, so further investigation is required.
- The approach used to analyze the liquid sheet breakup distance yielded that the sheets disturbance (i.e. instabilities) that introduces the disintegration process occurs at an early stage compared to the pure fuels.
- The highest point or the summit location found using the second order moment approach, showed that the nanofuel's liquid sheet breakup distances were shorter than the pure fuels' distances.
- The liquid sheet dynamics were displayed near the nozzle, and it was found that it changes as different concentration of MNP were added. Also, depending on the used base fuel, the dynamic behavior will change as well. This is a consequence of the altered evaporation characteristics due to the dispersion of the nanoparticles regardless of the used base fuel.
- The obtained data shows that the mean axial velocities of nanofuels were higher than the base fuels, for all cases studied here.

Each result presented above emphasize the effects of Aluminum Oxide nanoparticles dispersion in: conventional (Jet A-1), alternative (GTL), and mixture of both jet fuels, on the macroscopic properties of spray performance. The final findings are vitals as it helps to understand the effect of nanoparticles on the evaporation and combustion processes.

For future plans, the created nanofuels and their base fuels can be moved to the next stage where evaporation and combustion properties are studied.

REFERENCES

[1] Yang, J., Xin, Z., He, Q., Corscadden, K., and Niu, H., 2019, "An Overview on Performance Characteristics of Bio-Jet Fuels," Fuel, **237,** pp. 916-936.

[2] Stapels, M., Malina, R., Suresh, P., Mileman, J., and Barrett, S., 2018, "Aviation CO_2 Emissions Reductions from the Use of Alternative Jet Fuels," Energy Policy, **114**, pp. 342-354.

[3] Rashad, R., and Zingg, D., 2015, "Actions to Reduce the Climate Change Impact of the Aviation Sector," Ph.D. thesis, University of Toronto Institute for Aerospace Studies.

[4] Wang, W., and Tao, L., 2016, "Bio-Jet Fuel Conversion Technologies," Renewable and Sustainable Energy Reviews, **53**, pp. 801-822.

[5] Han, H., Kim, C., Cho, C., Sohn, C., and Han, J., 2018, "Ignition Delay Time and Sooting Propensity of a Kerosene Aviation Jet Fuel and Its Derivative Blended with a Bio-Jet Fuel," Fuel, **232**, pp. 724-728.

[6] Yilmaz, N., and Atmanli, A., 2017, "Sustainable Alternative Fuels in Aviation," Energy, **140**, pp. 1378-1386.

[7] Neuling, U., and Kaltschmitt, M., 2018, "Techno-Economic and Environmental Analysis of Aviation Biofuels," Fuel Processing Technology, **171**, pp. 54-69.

[8] Yu, W., Tay, K., Zhao, F., Yang, W., Li, H., and Xu, H., 2018, "Development of a New Jet Fuel Surrogate and Its Associated Reaction Mechanism Coupled with a Multistep Soot for Diesel Engine Combustion," Applied Energy, **288**,pp. 42-56.

[9] Liu, G., Yan, B., and Chen, G., 2013, “Technical Review on Jet Fuel Production,” Renewable and Sustainable Energy Reviews, **25**, pp. 59-70.

[10] P. Lobo, L. Rye, P.I. Williams, S. Christie, I. Uryga-Bugajska, C.W. Wilson, D.E. Hagen, P.D. Whitefield, S. Blakey, H. Coe, D. Raper, and M. Pourkashanian, Impact of Alternative Fuels on Emission Characteristics of a Gas Turbine Engine-Part 1: Gaseous and Particulate Matter Emissions, Environmental Science and Technology, 46, 10805-10811, 2012.

[11] Blaky, S., Tye, L., and Wilson, C., 2011, “Aviation Gas Turbine Alternative Fuels: A Review,” *Proceedings of the Combustion Institute,* **33**, 2010, pp. 2863-2885.

[12] Choudhury, P., 1992, “Slurry Fuels,” Progress in Energy and Combustion Science, **18**(5), pp. 409-427.

[13] Peleg, I., and Timnat, Y., 1982, “Combustion of Aluminum and Boron Slurry Fuels in a Dump Combustor,” *Symposium (International) on Combustion,* **19**(1), 1982, pp. 557-563.

[14] Gan, Y., and Qiao, L., 2011, “Combustion Characteristics of Fuel Droplets with Addition of Nano and Micron-Sized Aluminum Particles,” Combustion and Flame, **158**, pp. 354-368.

[15] Yetter, R., Risha, G., and Son, S., 2009, “Metal Particle Combustion and Technology,” *Proceedings of the Combustion Institute,* **32**, 2009, pp. 1819-1838.

[16] Hunt, E. M., and Pantoya, M. L., 2005, "Ignition Dynamics and Activation Energies of Metallic Thermites: from Nano- to Micron- Scale Particulate Composites," Journal of Applied Physics, **98**(3), p. 034909.

[17] Soudagar, M., Nik-Ghazali, N., Abul Kalam, M., Badruddin, I., Banapurmath, N., and Akram, N., 2018, “The Effect of Nano-Additives in Diesel-Biodiesel Fuel Blends: a Comprehensive Review on Stability, Engine Performance and Emission Characteristics,” Energy Conversion and Management, **178**, pp. 146-177.

[18] Sonawane, S., Patankar, K., Fogla, A., Puranik, B., Bhandarkar, U., and Sunil Kumar, S., 2011, "An experimental Investigation of Thermo-Physical Properties and Heat Transfer Performance of Al2O3-Aviation Turbine Fuel Nanofluids," Applied Thermal Engineering, **31**(14), pp. 2841-2849.

[19] Sonawane, S., Bhandarkar, U., Puranik, B., and Kumar, S. S., 2012, "Convective Heat Transfer Characterization of Aviation Turbine Fuel-Metal Oxide Nanofluids," Journal of Thermophysics and Heat Transfer, **26**(4), pp. 619-628.

[20] Yue, L., Lu, X., Chi, H., Guo, Y., Xu, L., Fang, W., Li, Y., and Hu, S., 2014, "Heat-Sink Enhancement of Decalin and Aviation Kerosene Prepared as Nanofluids with Palladium Nanoparticles," Fuel, **121**, pp. 149-156.

[21] Javed, I., Baek, S. W., and Waheed, K., 2014, "Effects of Dense Concentrations of Aluminum Nanoparticles on the Evaporation Behavior of Kerosene Droplet at Elevated Temperatures: The Phenomenon of Microexplosion," Experimental Thermal and Fluid Science, **56**, pp. 33-44.

[22] Javed, I., Baek, S. W., and Waheed, K., 2015, "Autoignition and Combustion Characteristics of Kerosene Droplets with Dilute Concentrations of Aluminum Nanoparticles at Elevated Temperatures," Combustion and Flame, **162**(3), pp. 774-787.

[23] Javed, I., Baek, S. W., Waheed, K., Ali, G., and Cho, S. O., 2013, "Evaporation Characteristics of Kerosene Droplets with Dilute Concentrations of Ligand-Protected Aluminum Nanoparticles at Elevated Temperatures," Combustion and Flame, **160**(12), pp. 2955-2963.

[24] Kim, D. M., Baek, S. W., and Yoon, J., 2016, "Ignition Characteristics of Kerosene Droplets with the Addition of Aluminum Nanoparticles at Elevated Temperature and Pressure," Combustion and Flame, **173**, pp. 106-113.

[25] Ghamari, M., and Ratner, A., 2017, "Combustion Characteristics of Colloidal Droplets of Jet Fuel and Carbon-Based Nanoparticles," Fuel, **188**, pp. 182-189.

[26] E, X., Zhi, X., Zhang, X., Wang, L., Xu, S., and Zou, J.-J., 2018, "Ignition and Combustion Performances of High-Energy-Density Jet Fuels Catalyzed by Pt and Pd Nanoparticles," Energy & Fuels, **32**(2), pp. 2163-2169.

[27] Soltan, M., Al Abdulla, B., Al Dosari, A., Kannaiyan, K., and Sadr, R.,2018, "Spray Performance of Alternative Jet Fuel Based Nanofuels at Hight-Ambient Conditions," *International Mechanical Engineering Congress and Exposition*, 2018, 7, doi:10.1115/IMECE2018-87387

[28] Hwang, J., Park, Y., Bae, C., Lee, J., and Pyo, S., 2015, "Fuel Temperature Influence on Spray and Combustion Characteristics in A Constant Volume Combustion Chamber (CVCC) Under Simulated Engine Operating Conditions" Fuel, **160**, pp. 424-433.

[29] Krishnaraj, J., Vasanthakumar, P., Hariharan, J., Vinoth, T., and Karthikayan, S., 2017, "Combustion Simulation and Emission Prediction of Different Combustion Chamber Geometries Using Finite Element Method," *Materials Today: Proceedings*, **4**(8), 2017, pp. 7903-7910.

[30] Mohamed Soltan, Buthaina Abdulla, AlReem AlDosari, Kumaran Kannaiyan and Reza Sadr, (2019) "Effect of Nanoparticles on Alternative Fuel Sprays at High-Pressure Conditions," Final technical report submitted to QNRF.

[31] Lefebvre AH. Fifty years of gas turbine fuel injection. Atomization Sprays 2000;10(3–5):251–76.

[32] Kannaiyan, K., and Sadr, R., 2017, "The Effects of Alumina Nanoparticles as Fuel Additives on The Spray Characteristics of Gas- To-Liquid Jet Fuels," Experimental Thermal and Fluid Science, **87**, pp. 93-103.

[33] Payri, R., Salvador, F., Gimeno, J., and Novella, R., 2011, "Flow Regime Effects on Non-Cavitating Injection Nozzles Over Spray Behavior," International Journal of Heat and Fluid Flow, **32**(1), pp. 273-284.

[34] Shariatmadar, F. S., and Pakdehi, S. G., 2017, "Synthesis and characterization of aviation turbine kerosene nanofuel containing boron nanoparticles

[35] Keane, R. D., and Adrian, R. J., 1992, "Theory of cross- correlation analysis of PIV images," Applied Scientific Research, 49(3), pp. 191-215.

[36] Meinhart, C. D., Wereley, S. T., and Santiago, J. G., 2000, "A PIV Algorithm for Estimating Time-Averaged Velocity Fields," Journal of Fluids Engineering, 122(2), pp. 285-289.

[37] Lefebvre, A. H., 1989, Atomization and Sprays, First Edition, CRC Press, USA

[38] Benedict, L. H., and Gould, R. D., 1996, "Towards better uncertainty estimates for turbulence statistics," Experiments in Fluids, 22(2), pp. 129-136